Studies on EU-DEMO 3D coils requirements and conceptual design for error field correction and plasma control

Francesco Maviglia[a,b,*], Leonardo Pigatto[c], Fabio Villone[d], Hartmut Zohm[a,e], Christopher Albert[f], Pierluigi Bruzzone[g], Rico Buchholz[f], Ben Drumm[h], Jonathan Gerardin[i], Y.Q. Liu[l], Cesar Luongo[a], Mattia Siccinio[a,e], Sven Wiesen[a,m]

[a]*EUROfusion – Programme Management Unit, Boltzmannstrasse 2, 85748 Garching, Germany*
[b]*Associazione EURATOM-ENEA sulla Fusione, C.R. Frascati, C.P. 65-00044 Frascati, Rome, Italy*
[c]*Consorzio RFX, Corso Stati Uniti 4, Padova, 35127, Italy*
[d]*Consorzio CREATE, Univ. Napoli Federico II - DIETI, 80125 Napoli, Italy*
[e]*Max-Planck-Institut für Plasmaphysik, Garching, Germany*
[f]*Institute of Theoretical and Computational Physics, Technische Universität Graz, 8010, Austria*
[g]*Ecole Polytechnique Fédérale de Lausanne (EPFL), Villigen-PSI, CH-5232, Switzerland*
[h]*CCFE, Culham Science Centre, Abingdon, Oxon, OX14 3DB, UK*
[i]*CEA, IRFM, F-13108 St Paul-Lez-Durance, France*
[l]*General Atomics, PO Box 85608, San Diego, CA 92186-5608, USA*
[m]*Forschungszentrum Jülich, Institut für Energie - und Plasmaphysik, 52425 Jülich, Germany*
**Corresponding author: francesco.maviglia@euro-fusion.org*

This work presents the initial studies on the requirements for the design of 3D coils on EU-DEMO. The use of 3D coils in present machines includes two main purposes: the first one is the Error Field Correction (EFC). The EFC aims at minimizing the intrinsic non-axisymmetric fields in the machine. Fulfilling the requirements is evaluated with the minimization of residual error fields, both in vacuum and with plasma response. The second purpose relates to the application of 3D fields to control the plasma. The first of these control functions includes the manipulation of the locked neoclassical tearing modes (NTMs) phase, and their positioning in front of the electron cyclotron antennae, for optimum stabilization. A second function is the application of 3D perturbation of the plasma edge to suppress ELMs. As the fastest required time constant of the applied 3D fields is comparable or longer with respect to that of the vacuum vessel, ex-vessel coils can be considered. Another constraint considered, which is met in the finding of this work, is that the 3D fields applied do not generate 3D power exhaust effects, such as divertor lobes, that jeopardize the protection of the machine divertor/wall, in the case considered of the ELMs suppression. The aim of this work is to assess if one set of coils could be designed that fulfills all these purposes/functions. The results show that, by using ITER tolerances for the TF, CS and PF coils, all these functions on EFC (using the overlap criterion assumption, which includes the plasma response), NTM phase control and ELMs suppression can be met with the proposed design of one row of ex vessel coils. An additional activity has started to study if the non-resonant perturbations generated by this set of coils could lead to detrimental effects via neoclassical toroidal viscosity (NTV) torque. Preliminary considerations on the coil technology, are also presented, with no showstopper found in this preliminary phase.

Keywords: DEMO, 3D coils, plasma stability control, error field correction.

1. Introduction

It has been found in present tokamak experiments that the application of small 3-D fields by external coils (called here '3D coils') can significantly alter the plasma properties. For future devices, such coils can hence be foreseen in the design for optimization of plasma performance. In this contribution, we study the use of 3D coils for EU-DEMO [1]. It includes two main purposes: the first one is the Error Field Correction (EFC). The EFC aims at minimizing the intrinsic non-axisymmetric fields in the machine, rising from the tolerances on the magnets installations, and manufacturing, and from the machine intrinsic toroidal asymmetries, as the ports in the DEMO ferromagnetic breeding blanket, and the coils feeders. Those fields have generally low toroidal mode numbers, which at low plasma density may lead to the formation of locked modes and ultimately to disruptions. To reduce DEMO disruptivity, it is considered mandatory to use EFC for the reduction of residual error fields. The second purpose relates to the application of 3D fields to control the plasma. The first of these control functions, includes the manipulation of the phase of locked tearing modes, and their positioning in front of the electron cyclotron antennae, for optimum stabilization. A second control function is the application of 3D perturbation of the plasma edge to mitigate or suppress ELMs. As at present a fully suppressed or naturally ELM free regime is judged to be the only viable option for DEMO, this function depends on the option that will be ultimately chosen and developed. The third control function aims at tailoring the plasma rotation profile by inducing neoclassical toroidal viscosity (NTV), e.g. to facilitate the access to some ELM-free regimes (e.g. QH-mode), or to have an additional knob to control the plasma confinement, while at the same time making sure NTV will not have unwanted detrimental effects.

Another constraint considered for all the functional requirements desired, is that the 3D fields applied shall not generate 3D power exhaust effects, such as divertor lobes, that jeopardize the protection of the machine. As the fastest required time constant of the applied 3D fields is, for the NTM control ≈1s, *i.e.* comparable or longer with respect to the vacuum vessel time constant (≈ 500ms [2]), this allows the possibility to explore the use of ex-

vessel coils. The aim of this work is to assess if one set of coils can be designed to fulfil all these applications. Preliminary results and considerations on the coil technology, and maintainability are also presented.

2. Error Field Correction

The 3D error fields are due to unavoidable machine toroidal asymmetries coming from tolerances or by design. At the beginning of a discharge, at low density, or later in phases with high β, tokamak plasmas tend to amplify residual non-axisymmetric error fields, forming locked modes (tearing modes stationary in the laboratory frame). The most dangerous ones have toroidal mode numbers n=1 and may lead to disruptions. 3D perturbation coils can be used to cancel the residual error fields, reducing the danger of locked modes. The fulfilment of the EFC requirements, which is considered mandatory for DEMO, is evaluated with the minimization of residual error fields, both in vacuum and with plasma response.

2.1. Plasma response model with MARS-F code

Plasma response and penetration of external fields are known to be key aspects to understand the dynamics of error fields in Tokamaks and the possible impact on plasma stability [3]. A modelling workflow has been developed to evaluate the effect of error fields on the DEMO reference plasma. This workflow couples the equilibrium code CHEASE (axisymmetric high-resolution Grad-Shafranov solver) [4] with the stability code MARS-Q (linear resistive MHD solver with module for external fields) [5]. MARS-Q is used to obtain a plasma response model for a given equilibrium, through a set of numerical calculations in toroidal geometry. The OMFIT framework [6] is used to integrate the codes, develop, and execute the workflow. The adopted strategy is based on using an axisymmetric surface to couple plasma response fields with external perturbations, working in the Fourier space both poloidally and toroidally. The workflow produces a plasma response database to a generic set of independent vacuum perturbations. For each vacuum perturbation the so-called Equivalent Surface Current (ESC) procedure is applied, which is described in [7]. In this approach, the ESC is located at a given radial position $s = s_i$ (where s indicates the radial coordinate in MARS-Q and physically is the square root of the normalized poloidal flux) and is calculated as the solenoidal current which couples to a given radial field perturbation on a given control surface ($s = s_c$ with $s_i > s_c$). A mutual inductance matrix between radial field perturbation (B^1) and poloidal component of equivalent current (J^2) is calculated numerically in the Fourier space with fixed toroidal mode number (n) and a range of poloidal harmonics ($-34 < m < 34$):

$$B^1_m(s_c) = \sum_k M_{mk} J^2_k(s_i)$$

The surface current assumption implies that the radial component is $J^1 = 0$, thus the toroidal component J^3 can be calculated from the poloidal one (J^2) by using the divergence-free condition. The M matrix is then used to calculate equivalent surface currents for a set of independent radial field perturbation, these can be either single-m fields or perturbations rotating in space to cover the full poloidal angle. In the present work Gaussian-like unit perturbations with varying phase have been used. With the aforementioned ESC approach, a database of vacuum radial field perturbations and plasma response fields is calculated. This database, coupling Fourier harmonics of vacuum fields on the control surface to harmonics of plasma response in the plasma region, can be used to calculate in the Fourier space the plasma response to any external field that can be recovered with the given range of harmonics. The resulting database can be used for many purposes, including modelling of the response to error fields, and it can be exported and applied to external optimization workflows.

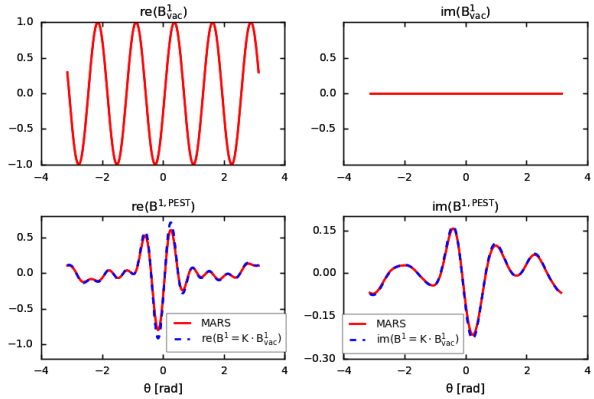

Figure 1 Comparison on reconstruction of plasma response (bottom row) to external fields (top row), calculated with the coupling matrix, versus a direct MARS run.

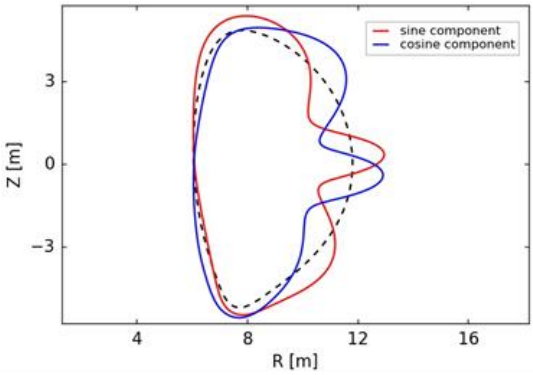

Figure 2 Components of the dominant mode from SVD of q=2 response coupling matrix

The physical model implemented for DEMO includes plasma resistivity but no toroidal flow, except a small constant value to ensure numerical robustness of the results. Plasma rotation however is known to have an influence on the screening of external fields; thus, it shall be considered in the future, once reliable predictions of the rotation expected in EU-DEMO are available. More than one strategy or physical metric can be adopted for EF correction. Two criteria have been considered for this DEMO case, starting with the cancellation (with EF correction coils) of the (m=2, n=1) resonant component of the total field (*i.e.* linear combination of vacuum and plasma response components). A coupling matrix has been calculated between Fourier harmonics of the vacuum fields and harmonics of the plasma response at the q=2 resonant surface.

$$B^{1,PLA}_m(s_{q=2}) = K\, B^{1,VAC}_m(s_c)$$
$$K = B^{1,PLA}_m(s_{q=2}) \cdot \left(B^{1,VAC}_m(s_c)\right)^{-1}$$

A cross-checking procedure has been adopted to test the capability of this coupling matrix of reproducing a given external field and the related plasma response. This implies using a generic external perturbation and comparing the plasma response obtained by applying the K matrix with those of direct MARS-Q runs. An example of the good achieved match is reported in Figure 1 for a sinusoidal vacuum field. This output can be applied to optimize EFC for cancellation of the m=2/n=1 resonant component of the total field, which is related to the most dangerous n=1 locked mode. As a second approach the so-called "overlap" criterion has been adopted. This technique, which is the one considered also by ITER [8], is based on compensating for those components of the external field the plasma is most sensitive to. These components are calculated with Singular Value Decomposition techniques from the plasma response model. In this case the global response is considered, over the whole plasma minor radius, and the right SVD matrix (V) is used to project the external field poloidal harmonics on the dominant mode of plasma response. Figure **2** shows an example of the sine-cosine components of the dominant mode for the DEMO case under investigation. To prevent EF penetration, the component that overlaps with the dominant field shall be reduced below a given threshold established with empirical scaling laws. Using a recent scaling [9] with DEMO parameters, reported in Table 1 (a full detailed list is in [10], Table 1, "EU-DEMO (QH-mode)" case).

I_p plasma current	18.27 MA
B_T Toroidal field at R	5.74 T
R plasma major radius	8.94 m
a plasma minor radius	3.1 m
k_{95} plasma elongation at 95%	1.65
l_i plasma internal inductance	1.02
β_p poloidal beta	1.04
q_{95} plasma safety factor at 95%	3.93
$\langle n \rangle / n_G$ Greenwald fraction	1.37

Table 1. Main DEMO plasma parameters used.

the threshold is found to be:

$$\delta_{n=1}^{ovlp} = {|B_{ovlp}|}/{B_T}$$

$$\leq 10^{-3.65\pm0.03} n_e^{0.58\pm0.06} B_T^{-1.13\pm0.07} R_0^{0.10\pm0.07} \left(\frac{\beta_N}{l_i}\right)^{-0.20\pm0.05}$$

$$\leq 1.1 \times 10^{-4}$$

Where the overlap field is calculated as the norm of the product between the first SVD mode and the external field harmonics, the latter taken on the aforementioned coupling surface s_c. In principle these could be taken directly on the plasma boundary, the coupling surface has been chosen however for consistency with the other applied metric and with the database calculation method. The surface is nevertheless close enough to the plasma boundary in terms of position and shape, so that the difference in the magnitude and Fourier spectrum of the vacuum field can be neglected.

2.2. 3D Electromagnetic error field calculations

Due to the lack of final detailed design of the DEMO magnetic cage, it was decided to consider only rigid perturbations, *i.e.* 6 shifts and tilts, for each of 27 active coils: 5 Central Solenoid (CS), 6 Poloidal Field (PF) coils, and 16 Toroidal Field (TF) coils (Figure 3). The vacuum magnetic field perturbation has been computed at the location of the ESC (Equivalent Surface Current) described above, for unit perturbations of the reference geometry, as follows:

- For TF coils, the CARIDDI code [11] has been used. A 3D mesh of the reference and perturbed geometries have been produced and the corresponding magnetic fields computed over the ESC, discretized with a suitable cloud of points denser where the coil is located, to improve accuracy (Figure 4). A mesh sensitivity analysis has been carried out to minimize the cancellation errors.
- For PF and CS coils, being the perturbation rigid, the coupling surface has been perturbed (*i.e.* shifted or tilted), while maintaining the nominal geometry for the coils (Figure 5). This way, the coils can be considered axisymmetric and analytical formulae can be used, hence retaining a very high accuracy. Cross-checks with numerical calculations have been carried out in sample cases.

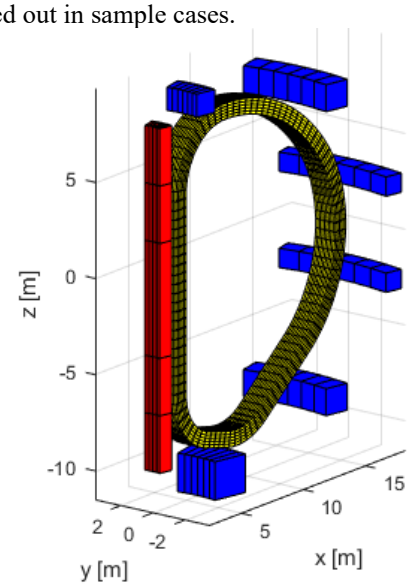

Figure 3 Toroidal section of the 3D model of the 5 CS, 6 PF, and 16 TF coils.

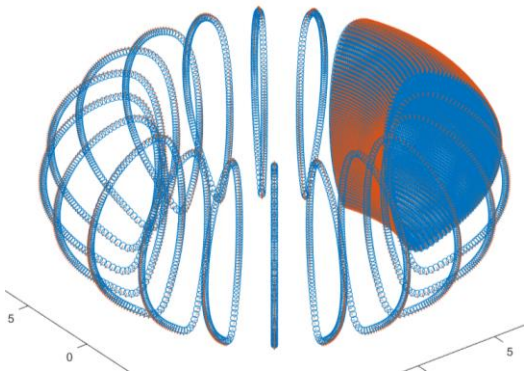

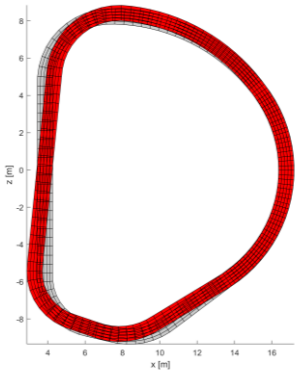

Figure 4 Top: discretization of the ESC for a TF coil located in the first sector. Bottom: 3D mesh of reference (gray) and perturbed (red) geometry (perturbation exaggerated)

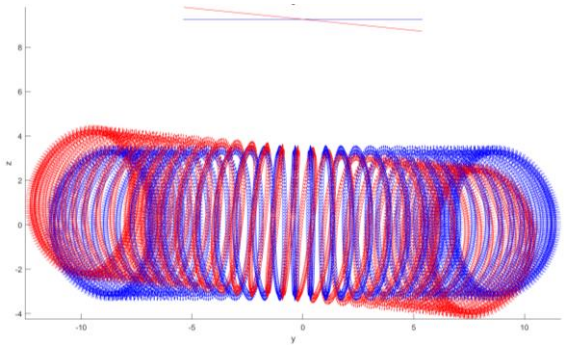

Figure 5 Sample perturbation (exaggerated) of the coupling surface

The geometrical perturbations of all coils have been assumed as random variables, uniformly distributed in intervals defined by the assumed tolerances. Due to the lack of final detailed design of DEMO coil system, it was decided to preliminarily use as perturbations the ITER values reported in [12]. A Monte Carlo analysis has been carried out, with a high number of samples in the explored set (10^6 – 10^8). For each sample of the set, the vacuum magnetic field perturbation due to the combination of the perturbations of all the coils has been computed over the ESC. Multiplying such vacuum magnetic field perturbation by the plasma response matrix described in the previous section, the corresponding overlap field B_{ovlp} defined above has been computed. Counting the number of occurrences in the explored set, the probability density function (pdf) of the overlap field can be recovered and the corresponding statistics (expected value, standard deviation etc.) can be computed (Table 2).

	10^6 samples	10^7 samples
Expected value E	2.68e-05	2.67e-05
Standard deviation σ	1.38e-05	1.38e-05
E + 3 σ	6.83e-05	6.82e-05
Worst case	1.11e-04	1.21e-04

Table 2 Statistics of the overlap field (normalized to reference toroidal magnetic field.

While the expected value and the standard deviation can be safely estimated also with a relatively low number of samples in the set, not surprisingly the worst case can be slightly underestimated. The worst case of the overlap field is above the threshold estimated in previous sections, *i.e.* 1.1×10^{-4}. In view of the uncertainties intrinsic in the estimate of the threshold and the possible underestimation of the worst case, it is mandatory to correct the error field using suitable Error Field Correction Coils (EFCC).

Three configurations of the EFCC have been investigated (Figure 6). Poloidally, only one EFCC is considered, almost symmetrical with respect to the z=0 plane, at three different radial positions (just outside the vacuum vessel, at the TF inner radial coordinate, at the outer TF radial coordinate). Toroidally, 16 such EFCC are considered, in the spatial region between two consecutive TF coils. These coils are supposed to be fed with a n=1 current of tuneable amplitude and toroidal phase.

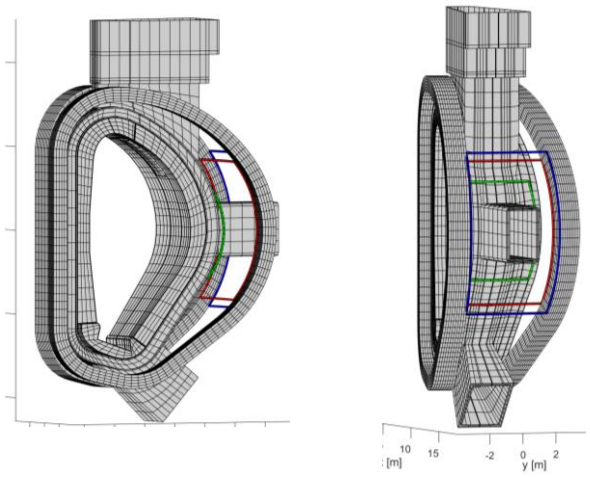

Figure 6 *Models of the 3 initial geometries considered for the EFCC: just outside the VV (green), at the inner radial coordinate of the TF (red), and at the outer radial coordinate of the TF (blue).*

The inner coils produce a higher magnetic field but with a broader spectrum. For each sample in the set of configurations, the optimal current and toroidal phase in the EFCC has been found as the one producing the minimum resulting overlap field when added to the original error field. Figure 7 reports the overlap field before and after such optimal correction, together with the current needed, for the EFCC located outside the TF coils.

Evidently, the correction is very effective and the current scales linearly with the overlap field to be corrected; even with a current saturation at 100kAturns, the resulting overlap field stays safely below the threshold. Surprisingly, the EFCC located on the vessel, closer to the plasma, are not equally effective, due to the broader poloidal spectrum giving rise to a cancellation when combined to the plasma response. The possible failure of EFCC has been investigated by introducing an additional random variable in the Monte Carlo analysis, indicating which coils are failing (i.e. with imposed zero current). The result is reported in Figure 8, which shows that up to 4 EFCC (out of 16) can fail, while still guaranteeing a reasonable margin with respect to the threshold. Similar computations have been carried out doubling the ITER tolerances considered [12]. All the results reported above scale linearly.

Applying the same computational chain to the vacuum field at the q=2 surface and computing the Three-Mode Error Index (TMEI) [13], instead of the overlap field, without the 3D coils, the resulting error is $\approx 6 \times 10^{-5}$, slightly above the threshold established for ITER (5×10^{-5}). The correction introduced by using the EFCC is very small, due to its localization in the poloidal plane.

The use of one poloidal set of coils only for EU-DEMO hence depends critically on the validity of the overlap criterion approach, which is considered the most update ITER criterion [8]. An additional activity has started to study if the non-resonant perturbations generated by this set of coils could lead to detrimental effects via neoclassical toroidal viscosity (NTV) torque.

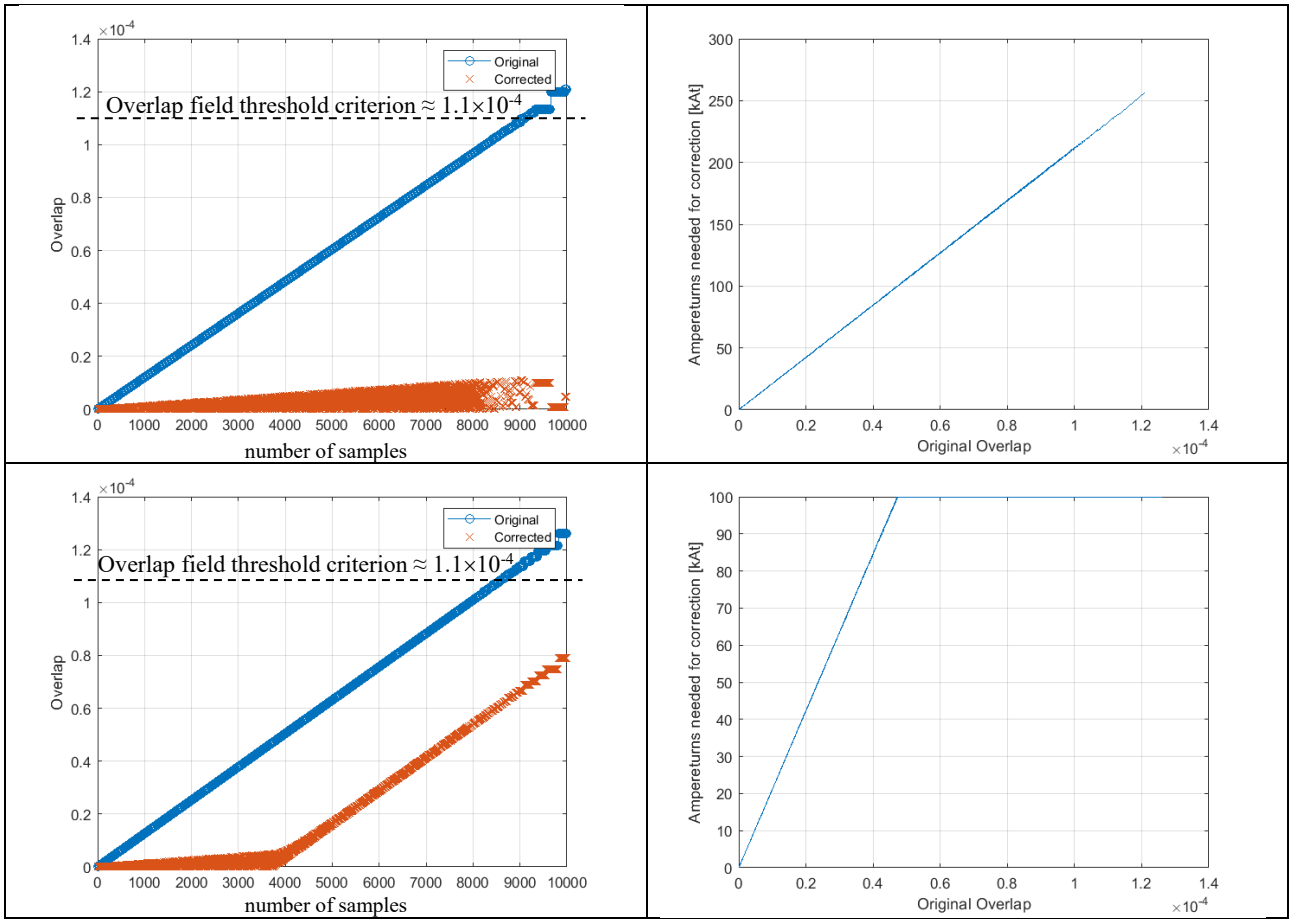

Figure 7 Correction with EFCC located outside the TF coils. Left: original vs. corrected overlap field, with the horizontal axis being equal to the number of random samples, sorted by the original "Overlap" increasing value. Right: corresponding current in EFCC. Lower row corresponds to a saturation current of 100kAturns in the EFCC

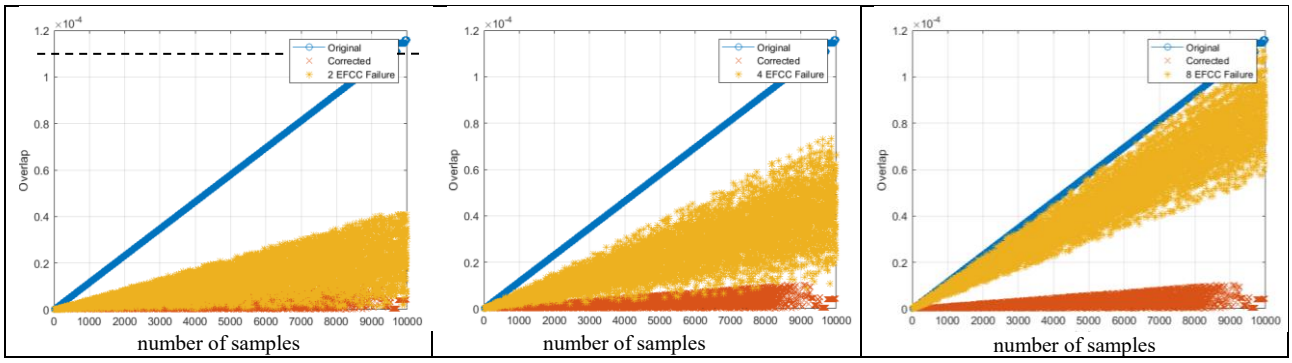

Figure 8 Effect of random failures of EFCC located outside the TF coils.

3. Control of the phase of locked tearing modes

The occurrence of tearing modes limits the operational space of tokamaks in density and radiative losses (in both cases triggered by the current gradient, 'classical' tearing modes) as well as achievable beta (pressure driven, 'neoclassical' tearing modes), with the islands occurring on resonant surfaces reducing the confinement, often also leading to disruptive termination of the discharge. A possible countermeasure is to drive local currents at the resonant surface by Electron Cyclotron Current Drive (ECCD), preferably in the O-point of the magnetic island **[14]**. In present day experiments, initially rotating tearing modes are often observed to lock in the laboratory frame, which is explained by a slowing down due to eddy currents induced in the vacuum vessel wall and then a phase locking to the helical component of the EF (see e.g. **[15]**). Since it is not guaranteed that the locked phase position is compatible with O-point injection through the ECCD launcher, it is proposed for future large tokamaks to use active coil sets producing helical components (Resonant Magnetic Perturbation, RMP) to move the locked mode into the optimum position for stabilization.

The principal feasibility of this scheme has been demonstrated experimentally in **[16]** and control has been discussed in **[17, 18]**. Here, we study the use of the 3D coils discussed above for this application.

A model is developed for this study and presented in [19], including momentum balance equation taking into account viscous drag, the force due to eddy currents in the wall and the force due to interaction with an external helical field. We chose a simple cylindrical geometry and neglect the toroidal component of the perturbed field. In this model, the mode interacts only with the component of the error field that has the same single helicity, so that the external field mimics both the error field as well as the (externally controlled) RMP field. The evolution of the island width is modelled by a modified version of the Rutherford equation, considering the effect of the RMP on the island width, but neglecting small island effects, since we are only interested in the locking of modes of appreciable size. The model expressions for the different terms can be found in [15]. For the application to DEMO, the input data for the error field are:

- an estimate of the error field on the q=2 surface due to imperfections in the TF, CS and PF coils.
- the optimized RMP field for compensation evaluated for the TMEI.

Both these inputs are derived by the calculation performed in the paragraph 2.2. They are combined into a single helicity component representing the compensated error field. We then use this field to simulate the forced rotation of tearing modes in DEMO. The 'average' compensated error field leads to a very low total island width $\widetilde{W}_{tot}$= 0.04 for which a mode of saturated island width $\widetilde{W}_{sat}$= 0.15 locks. In Figure 9, the temporal evolution of this case is shown. The mode frequency, in the upper left panel, drops to zero within 5 wall time constants τ_W (equal to ~500ms in the DEMO model used), indicating locking from then on. The upper right panel shows the mode amplitude, which saturates around that time to the value of $\widetilde{W}_{sat}$. The slight increase after locking is due to the destabilizing effect of the error field in the locking position. The lower left panel shows θ_0, the phase of the applied RMP field, which starts to increase linearly on a slow time scale at 20 τ_W to rotate the mode. The mode phase θ, shown in the lower right panel, follows the rotating RMP, on this timescale.

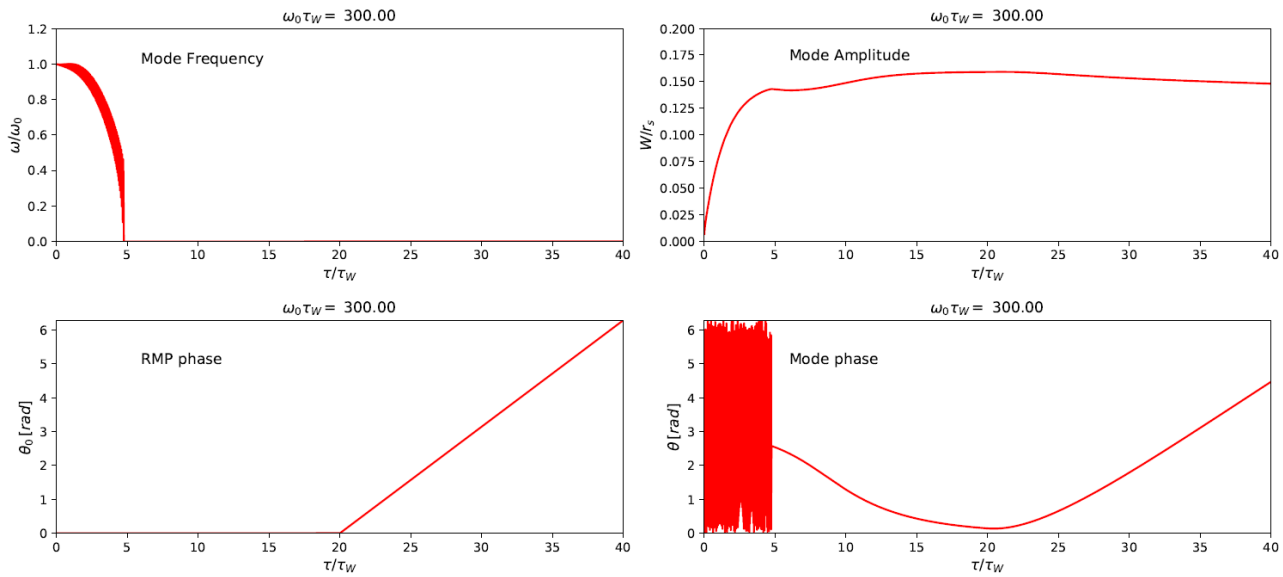

Figure 9 *Temporal evolution of mode frequency (upper left), mode amplitude (upper right), phase of the RMP field (lower left) and phase of the mode (lower right) for a case with a saturated mode amplitude of* $\widetilde{W}_{sat}$ *= 0.15, which locks to an RMP amplitude of* $\widetilde{W}_{tot}$ *= 0.04, At this amplitude, the mode can be moved around with by the RMP field (lower left).*

From the equation of motion in[19], the change of the mode phase can be estimated as

$$\tau_W \frac{d\theta}{dt} \leq 2\left(\frac{r_W}{r_s}\right)^{2m}\left(\frac{W_{tot}}{W}\right)^2$$

where θ is the phase angle of the mode of mode number m and island width W, W_{tot} is the width of the vacuum island produced by the applied 3D field and r_s and r_W are the radii of the resonant surface and the conducting wall, respectively. This indicates that the time scale of the process is given by the damping of eddy currents in the vessel wall and decreases with increasing ratio of RMP field to mode amplitude. Nonlinearly, if the RMP amplitude is too low, the mode will not rotate, but rather 'ratchet' through the rotating RMP field. We find that even for the low error field expected in DEMO, the mode will lock to the error field, but to move the mode on a typical time scale of tearing modes, the RMP amplitude required is exceeding that needed to compensate the intrinsic error field and thus sets the requirements. In this case, moving the mode on the time scale of 1 second (the typical reaction time of the ECCD system), an RMP coil current of 100 kAt is required for a mode amplitude of $\widetilde{W}_{sat}$ = 0.15 for the EFC coils positioned farther from the plasma, at the outer TF radial coordinate, studied here and for correcting the vacuum field according to the TMEI. In the worst case (opposite phase of intrinsic error field and ECCD launchers), this would add on top of the current needed to compensate the intrinsic error field.

4. ELM suppression or mitigation

A magnetic coil design study has been carried out in 2018 [20], for the purpose of mitigating or suppressing the

edge localized modes (ELMs) in an EU-DEMO reference scenario. The coil design, including both the coil geometry and the coil current requirement, is based on criteria derived from the linear, full toroidal plasma response computed by the MARS-F code [5]. With a single midplane row of coils, a coil size covering about 30°–50° poloidal angle of the torus is found to be optimal for ELM control using the n > 2 resonant magnetic perturbation (RMP) field (n is the toroidal mode number). With the same coil current, the ex-vessel coils can be made as effective as the in-vessel coils, at the expense of increasing the ex-vessel coils' size. This is however possible only for low-n (n = 1–3) RMP fields. With these low-n fields, and assuming 300 kAt maximal coil current, the computed plasma displacement near the X-point can meet the 10mm level, which was used as the conservative indicator for achieving ELM mitigation in EU DEMO. There are however large uncertainties on this number, so more detailed analysis is needed in the future to define more robust indicators for ELM suppression. Also, a single row of midplane coils will create non-resonant fields of opposite helicity, whose impact on the plasma will have to be assessed before it can be concluded that a single row of coils is sufficient. The risk of partial control coil failure in EU DEMO is also assessed based on toroidal modeling, indicating that the large n = 1 sideband due to coil failure may need to be corrected, if the nominal n > 1 coil configurations are used for ELM control in EU DEMO.

5. Evaluation of the impact of 3-D fields on power exhaust and first wall loads

An unwanted side effect of applied 3D fields could be the generation of lobes in the X-point region that may lead to 3-D effects in power exhaust. It was decided to study such effect, that may arise from the deliberate application of 3-D field for control purposes (i.e. for the NTM control, ELMs suppression, and NTV), on the heat power exhaust of the plasma facing components. This was done similarly to what has been evaluated for ITER, where the study of potential high heat flux "3D lobes" structures was reported in [21].

An initial evaluation was carried out for the case presented in paragraph 4, regarding the ELMs suppression or mitigation. 3D fields in vacuum have been produced for the n=1 to n=3 cases, with sinusoidal currents in the 16 3D coils considered for this study, with a peak current of 300kA. The 3D coil design considered is the one closer to the VV, to resemble as much as possible the previous DEMO study in [20]. The 3-D field was evaluated in vacuum, as an initial attempt, with the expectation of this being a conservative assumption, as the plasma is expected to partially damp these perturbations. This assumption must be verified/quantified in follow up studies.

A 3-D field line tracing routine was implemented to verify, starting from all the points of a grid, if some of the field line manage to escape the original unperturbed Last Closed Flux surface (LCFS). The results, shown in Figure 10, show the comparison of the unperturbed with the perturbed case. In the perturbed one, for the n=3 in this example, it is possible to notice the minimum psi-normalized (from the unperturbed case) reached starting from each point. The red color (for values <1) represent points which reach or originates from the region inside the original unperturbed LCFS (represented in white for values =1), while the blue points are from outside the unperturbed LCFS. Lobes are visible in both the strike points in the divertor area, detailed in Figure 11.

5.1. Field line tracing calculations on perturbed equilibrium

Backward field line tracing calculation was done, starting from all positions on the divertor. The field lines will enter the plasma core due to the perturbed equilibrium before exiting after several toroidal and poloidal turns. For each field line, the radial position reached on the outer mid-plane (OMP) the closest to the plasma centre is recorded. From SOLPS-ITER DEMO profiles [22] of electron density and temperature, shown in Figure 12, a parallel heat flux profile was defined ($q_{\parallel} \approx n_e \times T_e^{3/2}$).
The heat flux on the target is then equal to:

$$HF_{target} = q_{\parallel}(R_{OMP}) \times {R_{OMP}}\Big/{R_{target}} \times \sin\alpha \times q_0$$

With $q_{\parallel}$ the normalized parallel heat flux defined above, at the position R_{OMP}, R_{OMP} the radial position reached on the OMP (the closest one to plasma centre), R_{target} the radial position on the target, α the incident angle of the field line, q_0 a normalization factor so that the surface integral of the heat flux density on the divertor is equal to the injected power, as described in [23]. The comparison with the standard scenarios shows a much smaller maximum heat flux for the perturbed case and a larger wetted area, for both inner and outer divertor. Several lobes can be seen on the divertors. In Figure 13 is shown the inner divertor target.

A summary of the result is reported in the Table 3. This preliminary calculation was aimed at showing only the initial trends of the toroidal spreading of the heat flux on the PFC, rather than the absolute values, and if the "lobes" would reach areas outside the divertor. For future investigation more sophisticated codes must be employed to try to estimate the heat flux, and to add the plasma response to the 3D perturbation (as in the analyzed case a vacuum 3D perturbed field was superimposed to the axisymmetric case, neglecting how the plasma would respond, and re-arrange itself, due to the 3D perturbation). In the present literature is also shown that toroidal rotation of the heat flux pattern in the divertor may be necessary during the ELMs suppression (as it is planned in ITER [24]).
Additional calculation on the top of the tokamak were also done to verify the effect of the lobes at this location. With the current assumption of heat flux profile, the results are that the parallel heat flux carried by the field lines can be neglected.

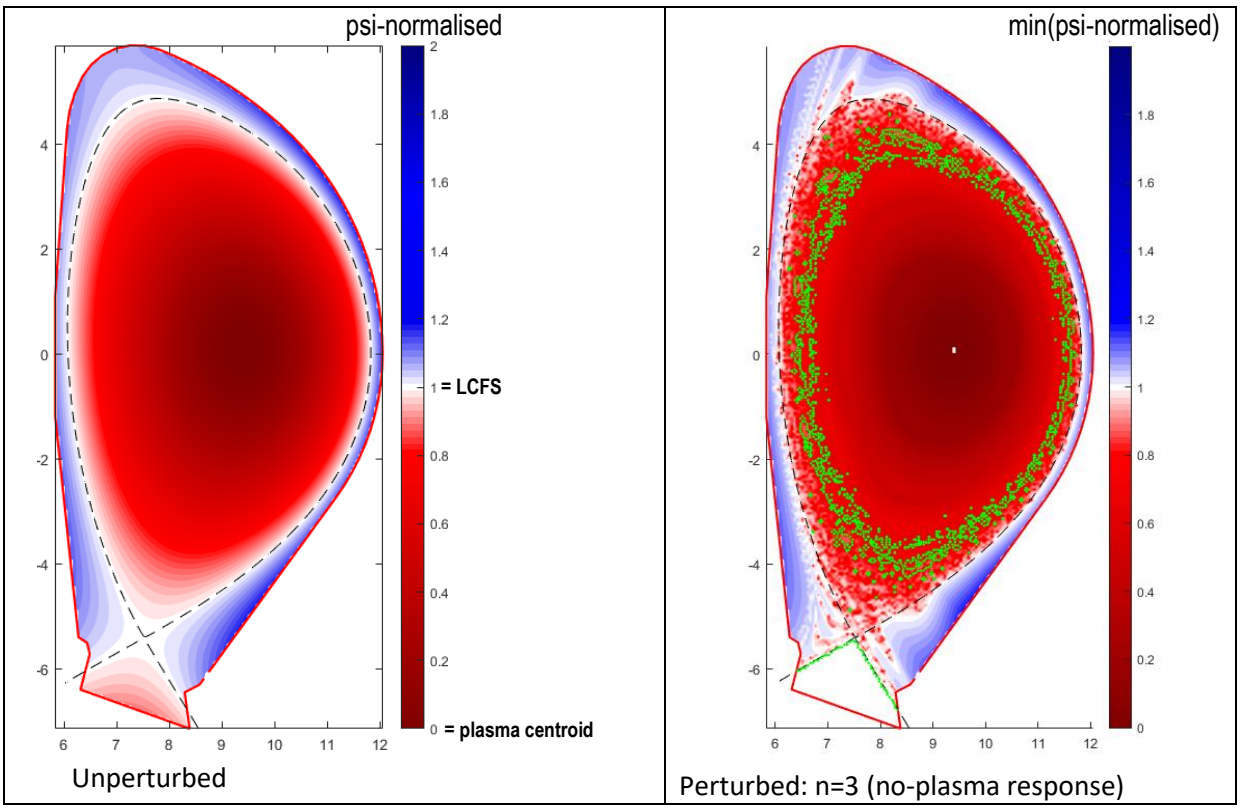

*Figure 10 Left figure: values of normalised psi for unperturbed case (colour code from *unperturbed case 0-**red**=plasma centroid, 1-white=LCFS, >1-**blue**= outside plasma). Right figure: Field line tracing showing min psi-normalized reached from each point using the colour code of the unperturbed case. The **green** points in the perturbed case represent points that do not escape from the plasma, and correspond to max reached psi_norm =1, i.e. the LCFS of the unperturbed case. In red are visible the lobes that may interact with the divertor or the upper first wall.*

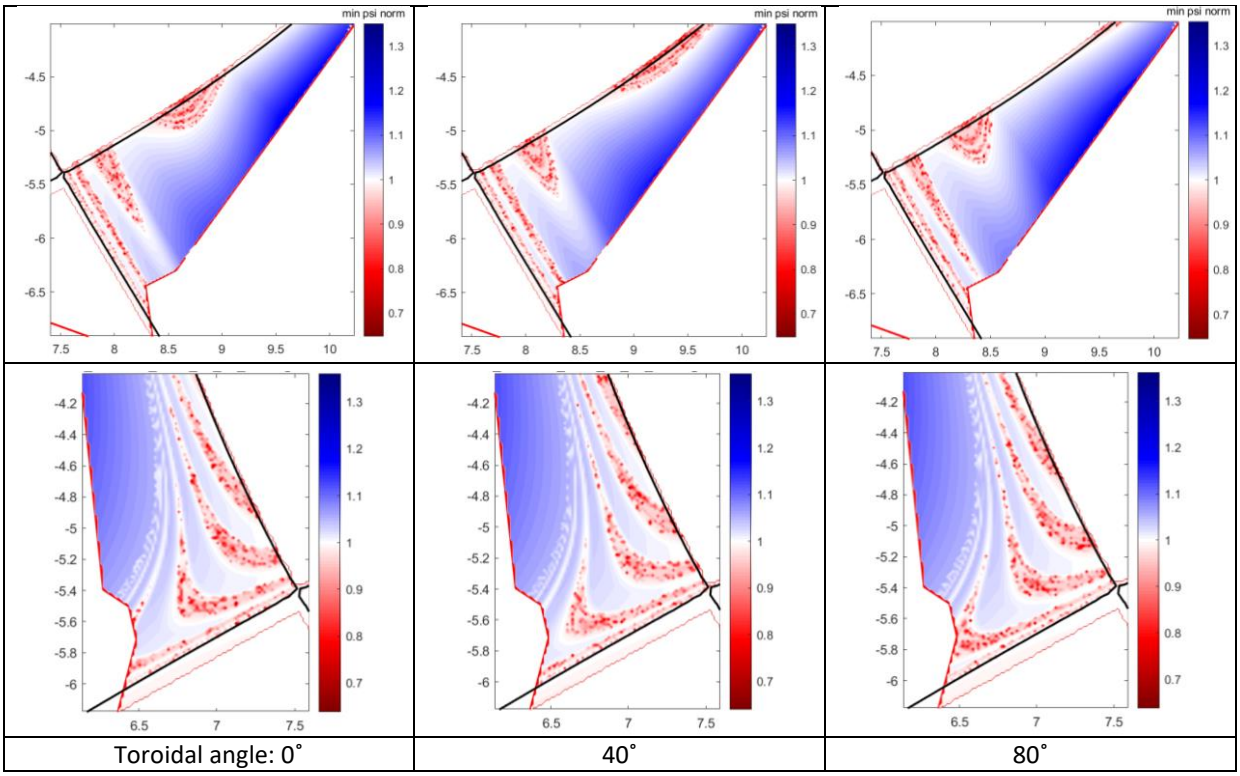

Figure 11. Details of divertor blobs (**red**) for the n=3 case, for several toroidal angles, for the outer (top) and inner target (bottom row).

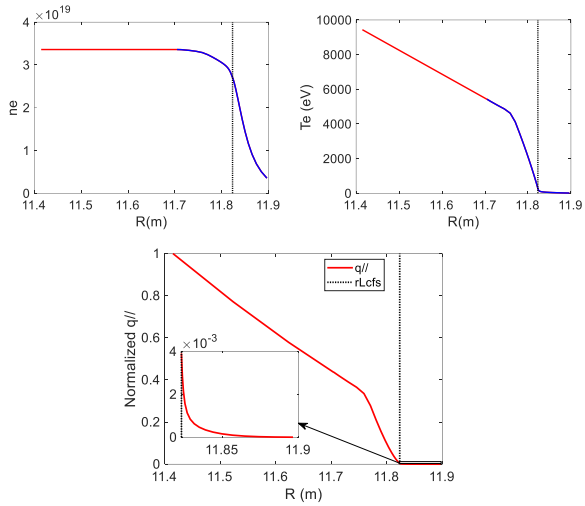

Figure 12 Electron density, electron temperature and estimated parallel heat flux at the OMP from SOLPS profiles (blue curve). Results were extrapolated towards plasma center to reach deeper position inside the plasma core (red part on the 2 figures of the left)

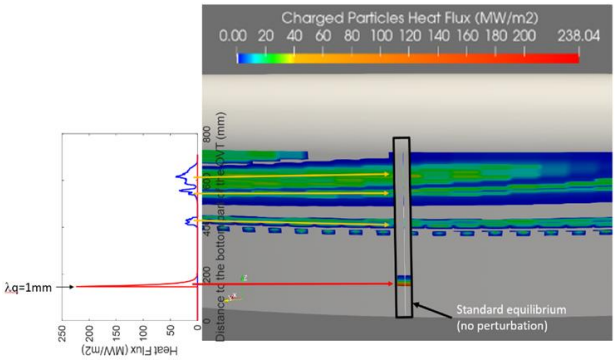

Figure 13 Example of heat flux density and wetted area for the standard (unperturbed) equilibrium (only a small toroidal fraction is shown in the black box, as it is an axisymmetric case), and the perturbed case in several toroidal positions.

Max HF (MW/m²)	Inner divertor		Outer divertor	
Max HF (MW/m²)	Inner divertor		Outer divertor	
	Unperturbed	Perturbed	Unperturbed	Perturbed
Vertical target	238	40	164	26
Rounded part	0	0	0	40
Wetted area (>1kW/m²) (m²)	**Inner divertor**		**Outer divertor**	
	Unperturbed	Perturbed	Unperturbed	Perturbed
Vertical target	2.2	23.6	3.0	13.8
Rounded part	0	0	0	7.2

Table 3 Tables summarizing the preliminary calculation evaluating: 1) on the top, the heat flux density in the SOF (unperturbed), and perturbed case, and 2) on the bottom, the wetted area.

6. Magnets technology options

A technology mapping exercise was carried out for the DEMO 3D coils to capture the trade-offs between coil technology (conductor), power consumption, and physics requirements. The main objective was to create a simple technology model to help in the decision of coil technology, specifically, if the DEMO 3D coils need to be superconducting or could be cryo-resistive (aluminum based) or even resistive (copper based). With certain simplifying, yet realistic, assumptions, the trade-off between physics requirements and power consumption can be captured by the simple expression:

$$\frac{(NI)^2}{\sqrt{A}} = 10^{-4}\frac{P}{\rho} \qquad \text{Equation 1}$$

In which NI are the required Amp-turns (from the physics mission), A is the area covered by an equivalent window-frame coil (related to its size), the factor 10^{-4} comes from a reasonable aspect ratio between coil thickness/coil window side (= 1/50), ρ is the resistivity of the material that makes the coil (for Cu at expected operating temperature of 423 Kelvin is equal to $2\text{x}10^{-8}$ Ωm, for Cryo-Al at 80 Kelvin is equal to $0.3\text{x}10^{-8}$ Ωm), and P is the power consumption, only for resistive, or cryo-resistive coils, while power consumption is approximated as zero for superconducting coils. In the case of cryo-cooled aluminum coil, the total power is composed of the resistive dissipation (as with Cu-resistive coils), plus the power needed to remove that dissipation from 80K to room temperature with an assumed (practical) fraction of Carnot efficiency. Many other simplifying assumptions are included in the constructive details of the 3D coils but Equation 1 captures in rough outlines the trade-offs among the major parameters.

Based on Equation 1, and using a typical size for a 3D coil of 10 m², the technology map can be sketched as shown in Figure 14. Two conductor options are shown, copper, at water operating-temperature of 423 K, and cryo-cooled aluminum operating at Liquid nitrogen temperature 80 K. Superconducting coils are nominally zero resistance and thus consume no power. For DEMO, we consider preliminarily a limit on the power consumption of 10 MW for the 3D coils. The physics mission requires the 3D coils to have between 150 and 300 kAmp-turns.

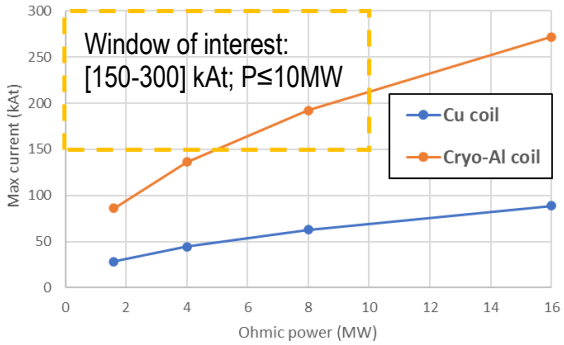

Figure 14 3D coil technology map for water operating temperature copper coils, and cryo-cooled aluminum coils.

The Cu-resistive coils cannot fulfill the physics mission within a reasonable power consumption limit. Cryo-resistive-Al coils can only partially meet the mission and cannot provide the maximum Amp-turns without exceeding maximum power limits. It can be concluded that the DEMO 3D coils have to be superconducting in order to meet the requirements, without exceeding consumption power limits. A corollary is that 3D coils cannot be easily replaced, and machine availability can only be assured through operational redundancy.

7. Conclusions and future work

In this paper are presented the initial studies on the requirements for the design of 3D coils on EU-DEMO. The functional requirements considered are the

corrections of the error fields, coming from toroidal asymmetries, and the application of 3D fields for plasma control (i.e. NTM phase control, ELMs suppression and tailoring of edge profiles via NTV). The aim of this work is to assess if one set of coils could be designed that provides all these functions. As the fastest required time constant of the applied 3D fields (≈1s for NTM control) is comparable or longer with respect to the vacuum vessel time constant (≈ 500ms [2]), this allows the possibility to explore the use of ex-vessel coils. A initial set of 16 ex-vessel coils (as per TF coils) is considered. These are located in the central outboard, and 3 alternative radial position were studied, i.e. just outside the vessel, at the TF inner radial coordinate, and at the outer TF radial coordinate.

The error field correction requirement was evaluated by using the TMEI [13], in vacuum, and the most update ITER criterion of the overlap field [9, 8], which include the plasma response. This requirement is judged to be mandatory, as it will greatly decrease the disruptivity of the machine and may relax the tolerance precision of the magnetic cage, which represent at present a large cost. The results show that, by using ITER tolerances for the TF, CS and PF coils, it is possible to correct the error field below the estimated DEMO threshold for the overlap field criterion, $B_{ovlp}/B_T \leq 1.1 \times 10^{-4}$, with all the 3 proposed set of coils. The EFCC at the outer TF radial coordinate are effective in fulfilling the criterion, while for the coils on the vessel a much higher current of the order of 1.4MAt is required, due to cancellation. Even with a failure of up to 4 EFCC the error field is still sufficiently corrected. This gives an initial indication on the minimum toroidal number of coils, which will need to be weighed against the redundancy to failure that may be required for these coils. The current required in the worst case is of the order of 250kAt, but also with 100kAt the limit is met. Finally doubling the ITER tolerances used here, the requirements will scale linearly. Applying the same computational chain to the vacuum field at the q=2 surface and computing the Three-Mode Error Index (TMEI) [13], instead of the overlap field, without the 3D coils, the resulting error is $\approx 6 \times 10^{-5}$, which is slightly above the threshold established for ITER (5×10^{-5}). The 3D coils design considered is rather ineffective in correcting the TMEI, due to its localization in the poloidal plane and the consequent poloidal spectrum. The use of one poloidal set of coils only for EU-DEMO hence depends critically on the validity of the overlap criterion approach, which is considered the most update ITER criterion.

Regarding the application of 3D fields for the NTM phase control, a model is developed for this study, including momentum balance equation taking into account viscous drag, the force due to eddy currents in the wall and the force due to interaction with an external helical field, detailed in [19]. The results shows that the time scale of the phase control is given by the damping of eddy currents in the vacuum vessel and decreases with increasing RMP field and mode amplitude. To move the mode on the time scale of 1 second (the typical reaction time of the ECCD system), an RMP coil current of 100 kAt is required for a mode amplitude of $\widetilde{W}_{sat}$= 0.15, for correcting the vacuum field according to the TMEI. In the worst case (180° misalignment wrt ECCD), this would add on top of the EFCC current. This was obtained for the coil option placed at the outer TF radial coordinate.

The results on ELMs suppression or mitigation, are based on [20]. The solution that was considered is the one of the central row of ex-vessel coils, with radial position similar to the first option of the Figure **6**, with radial position just outside the vacuum vessel. Assuming 300 kAt maximal current, this solution can achieve a plasma displacement near the X-point of around 10mm. This was the conservative indicator considered for achieving ELM mitigation in EU DEMO. This is however possible only for low-n (n = 1–3) RMP fields.

An initial evaluation of the effect on power exhaust by the application of 3D fields, was carried out on the ELMs suppression case mentioned above. This was done by superimposing an unperturbed 2D equilibrium with a n=1 to n=3 perturbations, as described in [20], in vacuum. 3D field line tracing routines have been implemented to verify the presence of lobes, which may escape the original unperturbed Last Closed Flux surface (LCFS). The results shows that the lobes remain confined within the divertor high heat flux capable targets and baffle areas. This study must be repeated in the future including the plasma response, to confirm the validity of the finding of this study.

Thus, the resonant helical spectrum generated by the 3D coil set studied here would be sufficient to fulfill the required control tasks. However, such a set of coils generates a significant amount of non-resonant perturbations (under fully symmetric conditions, the whole resonant spectrum will be accompanied by a spectrum of opposite helicity and same magnitude). These perturbations could lead to detrimental effects via neoclassical toroidal viscosity (NTV) torque. To study the NTV effects induced by external perturbations in DEMO, a new activity has started [25, 26]. This is aimed at making sure NTV will not have unwanted detrimental effects, while at the same time it can be used for tailoring the plasma rotation profile by NTV, e.g. to facilitate the access to some ELM-free regimes (e.g. QH-mode [27, 28]), or to have an additional knob to control the plasma confinement [29]. A workflow for NTV computation for a given magnetic configuration has been set up using a linear MHD model for the perturbed equilibrium (MARS-F/K) as well as on a 3D equilibrium VMEC for NEO-2 [30]/NEO-RT [31] based on a ripple test case. The next steps will be to perform and cross-verify simulations with MARS-Q (using the drift-kinetic module), NEO-2 and NEO-RT in the relevant regime. Results will show if more control of the poloidal spectrum is required, which would lead to the need for further rows of coils.

The final part presented the results regarding a technology mapping exercise for the DEMO 3D coils, to capture the trade-offs between coil technology (conductor), power consumption, and linking them with the functional requirements discussed. Three options were considered, *i.e.* resistive-Cu based coils, cryo-cooled Al based coils, and superconductive coils. Simplified assumptions were used on the 3D coils, combined with the electrical current needed for the physics requirement discussed, in a range from 150kAt to 300kAt, and with a preliminary power limitation defined as 10MW. The results shows that the resistive-Cu coils cannot fulfill the

requirements, while the Cryo-resistive-Al coils can only partially meet the mission and cannot provide the maximum Amp-turns without exceeding maximum power limits. It can be concluded that at present the preferred technology for EU-DEMO to meet the functional requirements without exceeding consumption power limits is to employ superconductive coils. A corollary is that 3D coils cannot be easily replaced, and machine availability can only be assured through operational redundancy.

Acknowledgments

This work has been carried out within the framework of the EUROfusion Consortium, funded by the European Union via the Euratom Research and Training Programme (Grant Agreement No 101052200 — EUROfusion). Views and opinions expressed are however those of the author(s) only and do not necessarily reflect those of the European Union or the European Commission. Neither the European Union nor the European Commission can be held responsible for them. The authors would like to thank the professor Raffaele Albanese, assistant professor Lidia Piron, and phd student Pasquale Zumbolo for their advice and expertise on 3D fields corrections.

References

[1] G. Federici et al, FED 2018, *https://doi.org/10.1016/j.fusengdes.2018.04.001.*

[2] F. Maviglia et al. FED 2018, *https://doi.org/10.1016/j.fusengdes.2019.01.127.*

[3] J. Park et al 2008 Nucl. Fusion 48 045006, *https://doi.org/10.1088/0029-5515/48/4/045006.*

[4] H. Lütjens, et al. Computer phys. comm. 97.3 (1996), *https://doi.org/10.1016/0010-4655(96)00046-X.*

[5] Y.Q Liu et al 2000 Phys. Plasma 7 3681, *https://doi.org/10.1063/1.1287744.*

[6] O. Meneghini et al 2015 Nucl. Fusion 55 083008, *https://doi.org/10.1088/0029-5515/55/8/083008.*

[7] Y.Q. Liu et al 2014 Plasma Phys. Control. Fusion 56 104002, *https://doi.org/10.1088/0741-3335/56/10/104002.*

[8] N.C. Logan, J.-K. Park, et al., "MDC-19 Updates for ITER Error Field Correction Criteria," in *41st MHD, Disruptions and Control TG Meeting*, IO, St Paul Lez Durance, France, 28 Mar - 31 Mar, 2023.

[9] N.C. Logan et al 2020 Nucl. Fusion 60 086010, *https://doi.org/10.1088/1741-4326/ab94f8.*

[10] M. Siccinio, et al. FED 2022, *https://doi.org/10.1016/j.fusengdes.2022.113047.*

[11] R. Albanese, et al. (1998) Adv. Imag. Electron. Phys., *https://doi.org/10.1016/S1076-5670(08)70121-6.*

[12] Y. Gribov et al., ITER/P5-9, *http://www-naweb.iaea.org/napc/physics/FEC/FEC2012/papers/154_ITRP529.pdf.*

[13] J. Knaster et al. FED 2011, *https://doi.org/10.1016/j.fusengdes.2011.02.045.*

[14] H. Zohm et al 1999 Nucl. Fusion 39 577, "DOI 10.1088/0029-5515/39/5/101".

[15] H. Zohm, MHD Stability of Tokamks, Weinheim: Wiley VCH., 2014.

[16] F.A. Volpe, et al., PRL, 2015., *https://doi.org/10.1103/physrevlett.115.175002.*

[17] W. Choi et al 2018 Nucl. Fusion 58 036022, *https://doi.org/10.1088/1741-4326/aaa6e3.*

[18] K.E.J. Olofsson et al 2016 PPCF 58 045008, *https://doi.org/10.1088/0741-3335/58/4/045008.*

[19] H. Zohm (2022). Report IPP 2022-06., *http://hdl.handle.net/21.11116/0000-000B-1BBE-2.*

[20] L. Zhou et al 2018 Nucl. Fusion 58 076025, *https://doi.org/10.1088/1741-4326/aac602.*

[21] H. Frerichs et al. Phys. Rev. Lett. 125, 155001 (2020), *https://doi.org/10.1103/PhysRevLett.125.155001.*

[22] F. Subba et al 2021 Nucl. Fusion 61 106013, *https://doi.org/10.1088/1741-4326/ac1c85.*

[23] J. Gerardin, et. al., NME 2019, https://doi.org/10.1016/j.nme.2019.01.002.

[24] P.T. Lang et al 2013 Nucl. Fusion 53 043004, *http://dx.doi.org/10.1088/0029-5515/53/4/043004.*

[25] R. Buchholz et al, Journal of Physics: Conference Series 2397, 012012 2022), DOI 10.1088/1742-6596/2397/1/012012.

[26] Buchholz R,et al., "Neoclassical toroidal viscous torque due to 3D magnetic perturbations in EU-DEMO," in *Proceeding submitted to 49th EPS Conference on Plasma Physics, Mo_MCF79*, Bordeaux, 2023.

[27] K.H. Burrell et al 2020 Nucl. Fusion 60 086005, *https://doi.org/10.1088/1741-4326/ab940d.*

[28] A.M. Garofalo et al 2011 Nucl. Fusion 51 083018, *https://doi.org/10.1088/0029-5515/51/8/083018.*

[29] R.J. Hawryluk et al 2015 Nucl. Fusion 55 053001, *https://doi.org/10.1088/0029-5515/55/5/053001.*

[30] S.V. Kasilov, et al. 2014 Phys. Plasmas 21 092506, *https://doi.org/10.1063/1.4894479.*

[31] C.G. Albert, et al. 2016 Phys. Plasmas 23 082515, *https://doi.org/10.1063/1.4961084.*